Advances in Nano Research, *Vol. 18, No. 3 (2025) 253-264*
https://doi.org/10.12989/anr.2025.18.3.253

Analysis of the changes in microstructure, mechanical, and contact properties of multi-pass friction stir processed dp800 steel

Semih Mahmut Aktarer[1], Tevfik Küçükömeroğlu[2], Dursun Murat Sekban[3,4], Ecren Uzun Yaylacı[5], Murat Yaylacı[*6,7,8], Mehmet Emin Özdemir[9] and İrem Mirzaloglu[6]

[1]*Department of Automotive Technology, Recep Tayyip Erdogan University, 53020, Rize, Turkey*
[2]*Department of Mechanical Engineering, Karadeniz Technical University, 61100, Trabzon, Turkey*
[3]*Department of Marine Engineering Operations, Karadeniz Technical University, 61530, Trabzon, Turkey*
[4]*WMS Engineering Services Industry Trade Limited Company, 61080, Trabzon, Turkey*
[5]*Faculty of Fisheries, Recep Tayyip Erdogan University, 53100, Rize, Turkey*
[6]*Department of Civil Engineering, Recep Tayyip Erdogan University, 53100, Rize, Turkey*
[7]*Faculty of Turgut Kıran Maritime, Recep Tayyip Erdogan University, 53900, Rize, Turkey*
[8]*Murat Yaylacı-Luzeri R&D Engineering Company, 53100, Rize, Turkey*
[9]*Department of Civil Engineering, Cankiri Karatekin University, 18100, Çankırı, Turkey*

(*Received October 30, 2024, Revised February 25, 2025, Accepted February 27, 2025*)

Abstract. In this study, the friction stir process (FSP), which can be successfully applied to plate-type materials, was applied to DP800 steel in a varying number of passes (1, 2, and 3 passes), and the effects of the FSP on the microstructure, hardness, and strength values of the steel were examined. In addition, the changes in the strength values after the FSP were transferred to the finite element (FEM) and artificial neural network (ANN) based contact problem models, and the changes in the contact stress and areas were determined comparatively. As a result of the examinations, it was determined that there were significant reductions in grain sizes in the microstructure compared to the pre-processed material at all pass numbers after FSP. As a result, the hardness and strength values of the steel increased after FSP. FEM and ANN analyses revealed that maximum contact stress values increased after FSP due to higher strength, while contact area values decreased proportionally.
Keywords: contact problem; DP800 steel; friction stir process; mechanical properties; microstructure

1. Introduction

Although many different types of steel are used in the literature for different applications (Chandra *et al*. 2024, Tlija *et al*. 2024), the use of dual-phase steels is rapidly increasing due to the advantages they provide (Küçükömeroğlu *et al*. 2017, Darabi *et al*. 2017). Dual-phase (DP) steels are advanced high-strength steel created through regulated heating and cooling operations, with ferrite and martensite in the microstructure. It has good formability and high strength because it comprises ferrite and martensite phases in its microstructure. Because of these features, the usage of DP steels has grown in various industries, including machine components, building materials, automotive, and shipbuilding, particularly in recent years.

Increasing the strength value in DP steels is generally possible by increasing the ratio of martensite form in the structure. However, it is also known that this structure change negatively affects steel properties such as formability and weldability. Therefore to increase the strength values of such steels, using secondary severe plastic deformation (SPD) methods instead of increasing the ratio of the martensite phase is considered a good option. Severe plastic deformation (SPD) methods are applied to improve materials' mechanical and physical properties by reducing the grain size to the nanometer scale. Many different SPD methods are used in the literature to increase the strength values of steels (Wetscher *et al*. 2006, Huang *et al*. 2008, Hazra *et al*. 2011, Jamaati *et al*. 2014, An *et al*. 2016, Xue *et al*. 2016, Ghalehbandi *et al*. 2018, Müller *et al*. 2019, Demirtas and Sekban 2021, Sekban *et al*. 2024a). However, considering its applicability to high-strength steels and plate-type materials, it can be said that the friction stir process (FSP) process stands out among other SPD methods. FSP is a severe plastic deformation method in which a rotary tool applies heat and plastic deformation to the material's surface by friction to refine the microstructure. This method is used especially in surface modification and material improvement processes to reduce the material's grain size and improve its mechanical properties. It is known from the literature that many variables, such as tool parameters, number of applied passes, and tool geometry, significantly affect the structure formed after FSP (Amirafshar and Pouraliakbar 2015, Hashemi and Hussain 2015, Rathee *et al*. 2015, Adetunla and Akinlabi 2018, Senthilkumar *et al*. 2019, Tonelli *et al*. 2019, Bagheri and Abbasi 2020, Farooq *et al*. 2020).

In the literature, empirical formulas, finite element-based models, artificial neural networks (ANN)-based models, and experimental investigations are frequently carried out to solve material-based engineering problems

*Corresponding author, Professor, Ph.D.,
E-mail: murat.yaylaci@erdogan.edu.tr

ISSN: 2287-237X (Print), 2287-2388 (Online)

(Kolahchi *et al*. 2016, 2019, Al-Furjan *et al*. 2022a, b, c, Hajmohammad *et al*. 2021, Motezaker *et al*. 2021, Sekban and Ölmez 2021, Sekban *et al*. 2024b, Furjan *et al*. 2024a, b, 2025, Shan *et al*. 2025). On the other hand, FEM and ANN methods offer significant advantages due to their low cost, fast analysis capacity, and ability to obtain results consistent with experimental results (Ammarullah *et al*. 2023, Ammarullah 2025). When the literature is examined, it is seen that FEM analyses are used in many different engineering problems and are also frequently used in contact problems (Salaha *et al*. 2023, Tauviqirrahman *et al*. 2023, Lamura *et al*. 2024). Similarly, it can be seen that ANN is used in many fields (Keerthiveettil Ramakrishnan *et al*. 2024, Sen *et al*. 2024, Saravanan *et al*. 2025, Yılmaz *et al*. 2022).

The literature shows that the FSP process applied to many different steels generally causes a reduction in grain size and, as a result, increases in properties such as strength and hardness (Costa *et al*. 2014, Xue *et al*. 2016, Nene *et al*. 2017, Sekban *et al*. 2017, Arora *et al*. 2019, Abubaker *et al*. 2020, Merah *et al*. 2020). When examined specifically for DP steels, it was determined that the studies on increasing the strength of this steel with FSP were quite limited (Gotawala *et al*. 2020, Aktarer *et al*. 2019, 2024, Yilmaz *et al*. 2024). In addition to increasing the mechanical properties of steels, it is critical to understand how changes in steels used in structural parts that come into regular contact, such as DP steels, affect contact mechanics. No study in the literature investigates the changes in qualities such as contact stress and contact distances caused by modifying the mechanical properties of DP steels in the structures in contact. In this way, the study aimed to reveal the effect of multi-pass FSP on the mechanical properties of DP 800 steel, which has no example in the literature, and also to reveal the effects of changing mechanical properties on contact mechanics. In this study, FSP was applied to DP800 steel with varying numbers of passes (1, 2, and 3 passes) to investigate the effects on microstructure, hardness, and strength. Also, the changes in strength values were transferred to the finite element-based contact problem and these changes' effects on maximum contact stress and contact areas were examined comparatively. As a result of the examinations, it was determined that the hardness and strength values of the steel increased compared to the base material as a result of the/due to refining of the grain structure in all the changing pass numbers. On the other hand, while close hardness and strength values were reached after 1 and 2 passes of FSP, it was observed that after 3 passes, there was a significant increase in the hardness and strength values of the structure, and the elongation values decreased. In the finite element-based and ANN-based contact problem, where the changes in mechanical properties are transferred, it was determined that the maximum contact stresses increased in all cases after FSP, and the highest maximum contact stress was obtained in the model created with steel properties after 3 passes of FSP. Also, it was determined that the contact area values decreased slightly after FSP, and the lowest contact area values were reached in the structure modeled with steel, to which 3 passes of FSP were applied.

2. Experimental procedure

2.1 Material and friction stir process

This study used hot-rolled DP800 steel with a chemical composition of 0.062% C, 1.927% Mn, 0.132% Si, 0.02% Al, 0.018% Cu, 0.25% Cr, 0.02% Ni, 0.015% Mo, and the remainder Fe was used. FSP was applied to DP800 plates with dimensions of 200 mm × 50 mm × 1.5 mm in multi-pass (1, 2, and 3 passes), as shown in Fig. 1. During FSP, a tool made of WC with a 14-flat shoulder and a cylindrical stirrer pin with a diameter and length of 5 mm and 1.3 mm, respectively, was used. While 1600 rpm was selected as the tool rotation speed, the tool traverse speed was determined as 170 mm per minute. During FSP, the shoulder inclination angle of the tool was set to 2°, and the tool pressing force was kept constant at 6 kN. The peak temperature during FSP was measured at two points corresponding to the stir zone (SZ) and the heat-affected zone (HAZ) using a K-type thermocouple. The two thermocouples were placed in small holes drilled into the middle of the plate thickness. Time-temperature austenitization diagram predictions have been conducted using the JMatPro software (Java-based Materials Properties). An optical microscope (OM) and scanning electron microscope (SEM) were used to observe the microstructure of the samples before and after FSP. Metallography samples were removed perpendicular to the machining direction (Fig. 1), polished with standard techniques, and then etched in 2% Nital (2 ml. HNO3 + 98 ml. C2H6O) for 20 seconds. Hardness and tensile test samples were taken from the base material and the plate to which FSP was applied in varying pass numbers, as seen in Fig. 1. Vickers hardness measurement method was used in hardness tests which were carried out at room temperature using a load of 200 g and a waiting time of 10 s. Hardness measurements were made in horizontal and vertical directions in 250 µm steps on the plate where FSP was applied in varying pass numbers, and a hardness distribution map was prepared after FSP. In order to determine the effect of changing number of passes after FSP on strength and elongation values, tensile test samples with dimensions of 1.4 mm × 3 mm × 8 mm were removed from the plate in the positions shown in Fig. 1 and were subjected to tensile testing at room temperature at a strain rate of 5x10-4 s^{-1}. The average stress-strain values obtained as a result of tensile tests performed at least 3 times are given in the study.

2.2 Finite element method

Contact mechanics is a discipline that studies solids in contact with each other. Due to the breadth of the study area and the variety of problems encountered, there are many studies on this subject. Many different methods have been used in studies conducted to date. Analytical analysis has an important place in contact problems. However, in recent years, it has been observed that numerical analysis data and modeling have also come to the fore. At the point where today's technology has come, it is now possible to obtain results very close to experimental results by modeling with

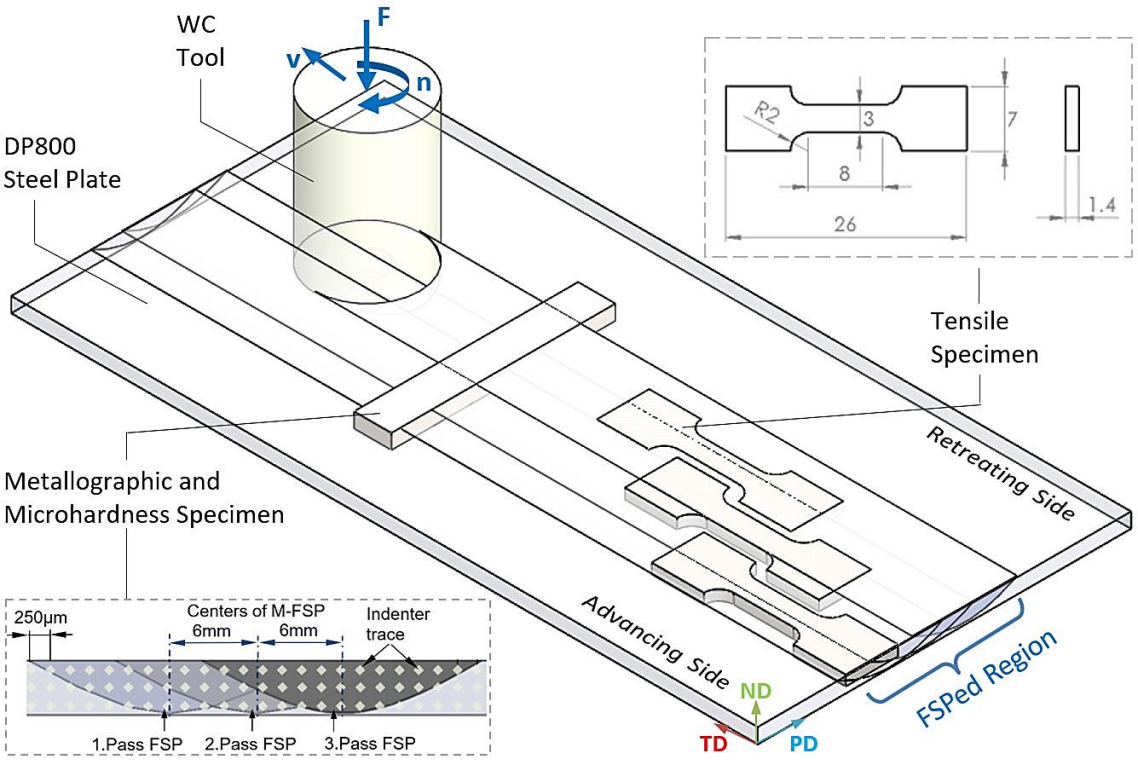

Fig. 1 Schematic representation of applied FSP and test samples

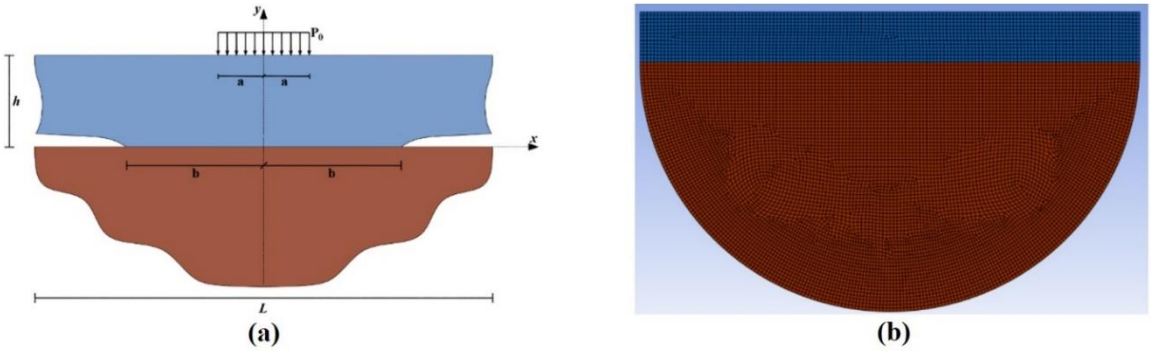

Fig. 2 ANSYS Workbench model of the problem: a) Solid model, b) mesh structure

advanced numerical analysis programs. In particular, software programs that adopt the Finite Element Method (FEM) provide realistic results by making the solution of complex engineering problems much more manageable (Yaylacı *et al*. 2024a, b, c, Wang *et al*. 2023, Wu 2023, Özdemir *et al*. 2024, Shen *et al*. 2024, Güvercin *et al*. 2025, Yemenoglu *et al*. 2025).

FEM is widely used by researchers in different disciplines to analyze stresses and strains in complex systems. The method creates a mathematical model for certain boundary conditions through differential equations. The designed mathematical model is divided into smaller elements and creates a mesh structure. Each element is connected with nodes to create a numerical model of the problem. The higher the number of elements in the mesh structure, the better the model behaves during analysis (Drai *et al*. 2023, Uzun Yaylacı *et al*. 2023a, b, Trung *et al*. 2023, Xia *et al*. 2023, Belabed *et al*. 2024, Daikh *et al*. 2024, Lafi *et al*. 2024, Sekban *et al*. 2024c).

ANSYS Workbench, a numerical analysis program, was used in this study. During the study, first, the geometry of the contact problem was determined, and a mathematical model was created in the ANSYS Workbench (2023 R1) program. Then, the element types were determined, and the material properties that formed the mathematical model were defined in the program. The contact problem geometry was studied with a layer and a half plane under the layer. The problem geometry and loading situation are seen in Fig. 2a. P_0, a known distributed load, acts symmetrically on the y-axis along the length (-a,+a). The layer and the half-plane are in contact in the (-b, +b) range along the length 2b. The material properties for the contact problem were determined as surface width L=1000 mm and surface thickness h=100 m, and all materials used were considered elastic and isotropic.

In the third stage, a mesh structure model was created with the selected elements of the mathematical model. The mesh structure model of the problem is shown in Fig. 2b.

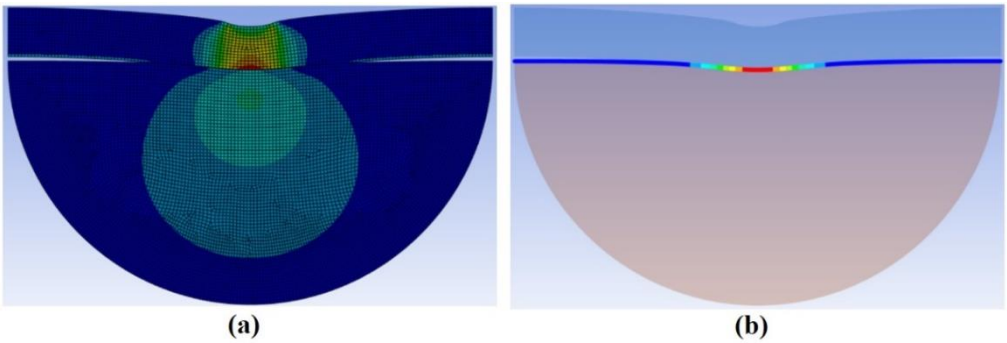

Fig. 3 Post-analysis images: a) Deformation shape, b) contact stress

Table 1 ANN test parameters

a (mm)			*p_0 (N/mm)*		
5	10	15	1000	1050	1100
20	25	30	1150	1200	1250
35	40	45	1300	1350	1400
50	55	60	1450	1500	1550
65	70	75	1600	1650	1700
80	85	90	1750	1800	1550
95	100	105	1900	1950	2000
5	10	15	1000	1050	1100

ANSYS Workbench program offers the opportunity to define mesh structures in different shapes based on the finite element method. The mesh structure of this contact problem model was created using the 2D-Quadrilateral - PLANE183 element with 4 corners and 8 nodes. Since the PLANE183 element has 2 degrees of freedom, it is very suitable for complex and irregular mesh structures. As a result of the experiments, the mesh structure of the problem was created by connecting 10441 elements with 31969 nodes. 586 CONTA172 and TARGE169 contact elements were used to define the contact area of the problem.

After creating the mesh structure, boundary conditions were determined, and loadings were defined ~~on~~/in the model. The deformation shape in the ANSYS Workbench model is seen in Fig. 3a. The contact problem was solved by determining the solution options. The results were examined using the determined boundary conditions, mesh structure, and element types. In the contact problem, the contact of the layer and half plane with the surface was studied. The friction between the punch and the surface was neglected, which was designed as a plane-strain problem. Fig. 3b shows the general contact stress image and focused image of the contact elements as a result of the ANSYS Workbench solution.

2.3 Artificial neural network

Artificial neural network-based techniques are used to solve nonlinear and complex relationships between data as an alternative to traditional regression models (Uzun Yaylacı 2024). In this study, the Broyden-Fletcher-Goldfarb-Shanno (BFGS) training algorithm was used with a feed-forward multilayer perceptron (MLP) to predict the contact stress and contact area. The training set for ANN was obtained from theoretical solutions (Table 1). The input layer of the network consists of two different parameters. These are as follows,

a (mm): Length of distributed load

p0 (N/mm): Applied distributed load

The output layer of the network consists of two parameters. This is as follows,

b (mm): Contact area

Pmax (MPa): Maximum contact stress

ANN model was employed in Statistica software 12 using the neural network module. The number of hidden layers and neurons were calculated by trial and error. The weights were assigned random values between 0.0001 and 0.001. Identity, logistic sigmoid, hyperbolic tangent, exponential, softmax, and Gaussian activation functions were tested, and 10000 networks were trained/retrained.

3. Results and discussions

3.1 The Temperatures in the FSPed Region

Temperatures in the processed region during FSP were monitored using thermocouples embedded in the plate. The peak temperatures in the SZ and HAZ reached 874°C and 400°C, respectively (Fig. 4a). SZ experienced heating rates of 170°C/s and cooling rates of 65°C/s. As shown in the TTA diagram in Fig. 4b, during FSP, the SZ is exposed to a temperature above the A3 temperature line. Therefore, the SZ was austenitized during FSP.

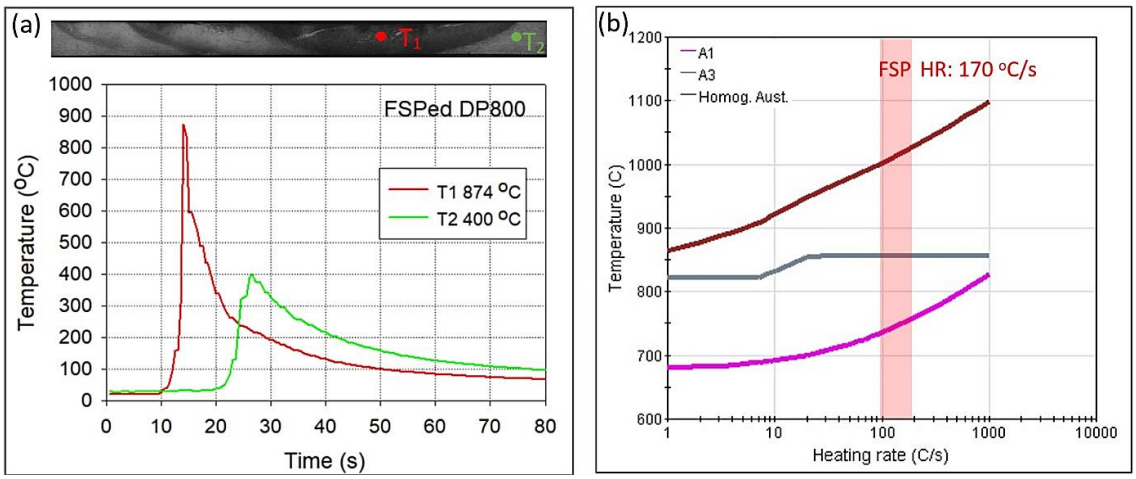

Fig. 4 (a) Temperature vs. time curves for the stir zone (SZ) and heat-affected zone (HAZ) during FSP, and (b) the time-temperature austenitization diagram (TTA) along with the corresponding heating rate (HR) during FSP

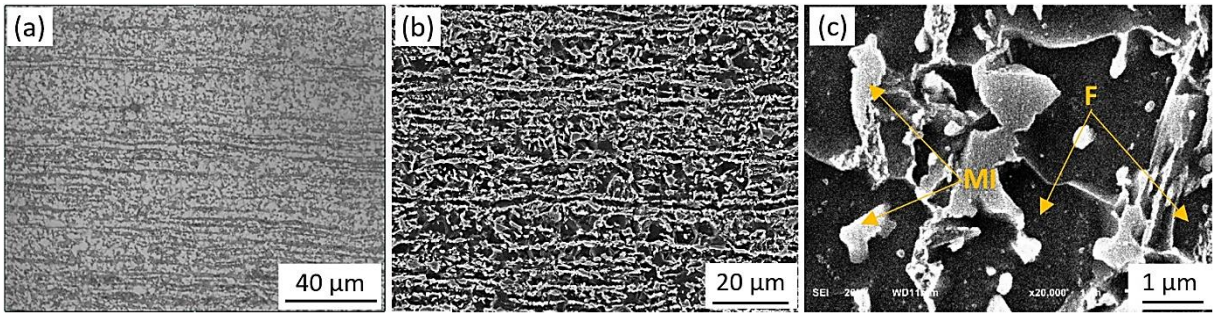

Fig. 5 The microstructure of the DP800 steel plate: (a) optical micrograph and (b) low and (c) high magnification SEM images

3.2 Microstructure

Optical and SEM micrographs showing the microstructures of DP800 steel plates are presented in Fig. 5. The initial microstructure of the DP800 steel sheet consists of ferrite (F) grains elongated in the rolling direction and martensite islands (MI) distributed along the ferrite grain boundaries. The average ferrite grain size is 4 µm, and the martensite volume fraction is approximately 44%. The martensite islands appear dark in the optical micrograph (Fig. 5a) and bright in the SEM image (Figs. 5b and 5c).

The optical micrograph of the region with multi-pass (M) -FSP is shown in Fig. 6a, and traces of the side-by-side pass are visible. After M-FSP, the heat-affected zone (HAZ), the thermomechanical-affected zone (TMAZ), and the stir zone (SZ) were typically observed in the processed zone (PZ). The microstructure of the first pass heat-affected zone is depicted in Figs. 6b and 6b1 exhibit a typical tempered martensite appearance partially decomposed into cementite and ferrite. Since the end of the TMAZ is the beginning of the HAZ, the lowest temperature of the TMAZ is the highest temperature of the HAZ. Therefore, it should be noted that the temperature in the HAZ is between the TMAZ temperature and approximately 400°C. The TMAZ temperature was not measured in this study, but it is known that the TMAZ temperature is slightly lower than the SZ temperature (Aktarer *et al*. 2019). Figs. 6c and 6c1 show the TMAZ of the first pass. The TMAZ consists of a very low fraction of ferrite lath, and island martensite. The temperature in this region is probably very close to the A3 temperature. During FSP, a very small volume of this region is ferrite, with most of it being austenite. Austenite transformed into martensite islands and lath during the subsequent cooling process, with ferrite remaining in the microstructure to a very low extent. Figs. 6d and 6d1 show the SZ of the first pass, which was influenced by the heat of the subsequent second pass. During FSP, depending on the temperature and cooling rate in the SZ, lath martensite is expected to form first. The microstructure of lath martensite was transformed into ferrite, martensite, and tempered martensite by the heat effect of the second pass. The microstructure shown in Figs. 6e and 6e1 are lath martensite. This region initially corresponded to the SZ of the first pass and then became the TMAZ of the second pass. Figs. 6f and 6f1 show the TMAZ of the first pass, followed by the SZ of the second pass, resulting in a final microstructure composed of refined equiaxed ferrite grains and martensite islands. Figs. 6g and 6g1 show the SZ of the second pass and the TMAZ of the third pass. The microstructure of this region is fine lath martensite. Figs. 6h and 6h1 show the SZ of the third pass, with the microstructure being lath martensite. In this region, the previous ferrite and martensite islands were transformed into austenite due to deformation and heat effect during FSP, resulting in lath martensite after cooling. Fig. 6i and 6i1 show the TMAZ of the third transition, with the microstructure of this region

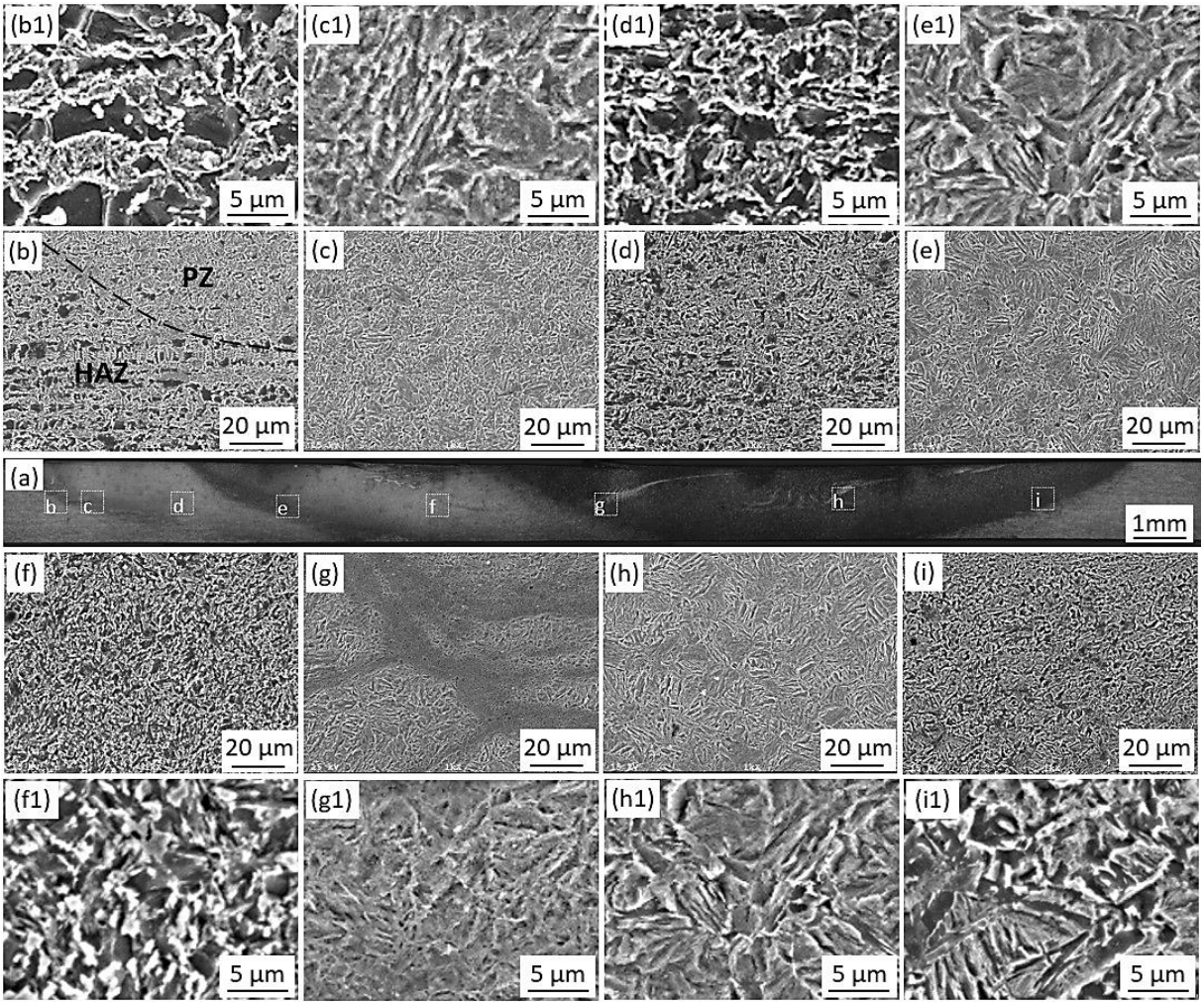

Fig. 6 (a) Optical micrograph of the cross-section of M-FSPed sample (b)-(b1) HAZ of the 1st pass, (c)-(c1) TMAZ of the 1st pass, (d)-(d1) SZ of the 1st pass, (e)-(e1) TMAZ of the 2nd pass, (f)-(f1) SZ of the 2nd pass, (g)-(g1), SZ of the 3rd pass in the advancing side, (h)-(h1) SZ of the 3rd pass, (i)-(i1) TMAZ of the 3rd pass

consisting of ferrite, bainite, and lath martensite. It is likely that during FSP, this region was exposed to temperatures just below the A3 temperature line. Some of this regions' ferrite and previous martensite islands transformed into austenite. Austenite transformed into lath martensite and bainite during the subsequent cooling process, while ferrite remained in the microstructure. Kang et al. reported that bainite and martensite microstructures can form in FSPed low alloy high-strength steel at different cooling rates (Kang *et al*. 2016). Their results showed that the microstructure was composed entirely of bainite at a cooling rate of 30 °C/s and predominantly martensite at a cooling rate of 70 °C/s. Similarly, Miles et al. reported observing lath martensite in the SZ of friction stir welded DP590 steel (Miles *et al*. 2006). In conclusion, the final microstructure in M-FSP processing depends on the initial microstructure, peak temperature, cooling rate, and deformation rate during the process.

3.3 Hardness

The microstructure image taken from the hardening area, the hardness distribution map created with the hardness values, and the hardness values taken both horizontally and vertically from the sample are shown in Fig. 7. As can be seen from the figure, the hardness value of 220 Hv in the base material increased in the areas affected by the tool after the application of FSP in all changing passes and reached 440 Hv level in the part of the sample where 1 pass FSP was applied, 450 Hv level in the part where 2 passes FSP was applied and 560 Hv level in the part where 3 passes FSP was applied. The hardness values increase compared to the base material in all the changing passes because of the grain refinement in the microstructure after FSP (Sekban *et al*. 2015). On the other hand, the significant decrease in grain size after 3 passes compared to 1 and 2 passes caused the hardness values to increase significantly after 3 passes compared to the FSP in the other passes. When Fig. 7c is examined, it is seen that in FSP performed side by side, the hardness values in the 1-2 pass intermediate zone and 2-3 pass intermediate zones show a tendency to decrease. This situation is because the grains tend to be coarse in these regions where the stirrer pin does not affect them, but the temperature rises. When Fig. 7d is examined, it is seen that similar hardness values occur in all pass numbers in part close to the surface. As you go down,

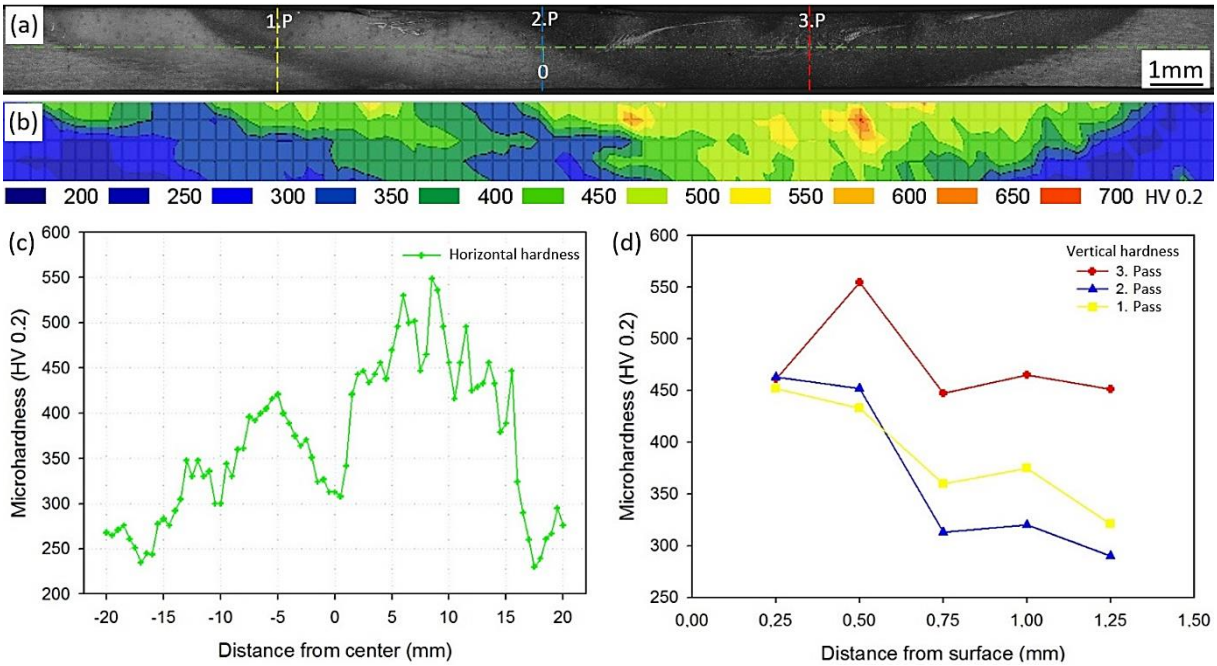

Fig. 7 (a) Optical microscope image of microstructure formed in the sample removed perpendicular to the multi-pass FSP direction, (b) hardness distribution map created with the hardness values measured based on this microstructure, (c) hardness values obtained horizontally in the extracted hardness sample, and (d) variation of hardness values downwards from the sample surface

Table 2 Tensile properties of base and varying number of passes FSP applied samples

Condition	Yield Strength (MPa)	Tensile Strength (MPa)	Uniform Elongation (%)	Total Elongation (%)	Toughness (Joule)
Base	567±11	829±14	14.9±0.5	23.5±1.1	4.82
1 pass FSP	803±14	968±18	6.8±0.7	15.4±0.9	3.49
2 pass FSP	907±13	1038±20	4.3±0.4	12.9±0.7	3.85
3 pass FSP	1221±16	1407±22	3.2±0.5	10.9±0.8	4.89

the hardness values where 3 passes of FSP are applied are obtained higher than the regions where 1 and 2 passes of FSP are applied. The hardness values in the near-surface part after 3 passes of FSP are close to those in other passes because the temperature in these regions increases due to the impact of the stirring pin and shoulder on the surface (Sekban *et al*. 2017). Since there was partial grain coarsening in the surface region, whose temperature increased significantly during the 3-pass FSP, the hardness values remained at a relatively low level. On the other hand, as one descends from the surface, the grain size decreases due to the effect of the stirring pin, causing the hardness values to increase significantly in these parts.

3.4 Strength and elongation

Fig. 8 shows stress-strain curves of the base and a varying number of passes FSP applied samples. On the other hand, the yield strength, tensile strength, uniform elongation, and total elongation values obtained from this curve for all conditions are given in Table 2. As can be seen, the yield and tensile strength values of 567 MPa and 829 MPa in the base material increased to 803 MPa and 968 MPa after 1 pass of FSP, to 907 MPa and 1038 MPa after 2 passes of FSP, and to 1221 MPa and 1407 MPa after 3 passes of FSP. On the other hand, the 15% uniform elongation value obtained in the pre-process samples decreased to 6.8% after 1 pass of FSP, 4.3% after 2 passes of FSP, and 3.2% after 3 passes of FSP. The increase in strength values and decrease in elongation values in all pass numbers after FSP are related to grain refinement in the microstructure (Hajian *et al*. 2015). As it is known, the decrease in grain size causes an increase in grain boundaries, which prevents the movement of dislocations. Therefore, it is possible to say that both the increase in strength values and the decrease in elongation values after FSP are due to this limitation in the movements of dislocations due to the decrease in grain size. On the other hand, it can be seen from the curve and table that the strength values increased significantly after 3 passes compared to the strength values obtained after 1 and 2 passes. The main reason for this situation is that the grain size in the microstructure after 3 passes of FSP decreases significantly compared to after 1 and 2 passes of FSP.

3.5 Contact mechanics analysis with FEM and ANN

Following the implementation of FSP on variable passes,

Table 3 Characteristics of ANNs that recognize output elements

Network name	Learning Error (%)	Testing Error (%)	Validation error (%)	Learning algorithm	Error function	Hidden activation	Output activation
MLP 2-11-2	0.08	2.11	0.89	BFGS 435	sos	Exponential	Identity
MLP 2-14-2	0	0.56	0	BFGS 273	sos	Logistic	Identity

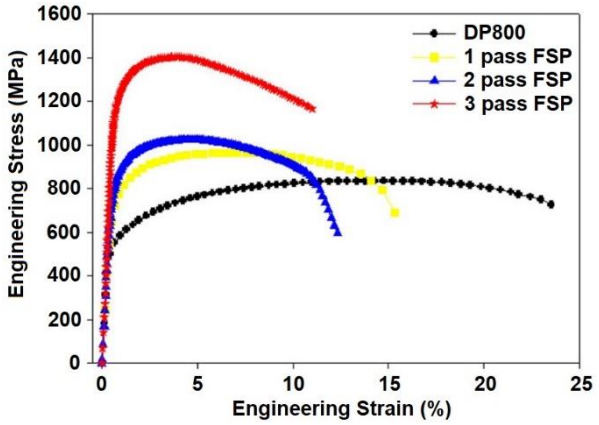

Fig. 8 Stress-strain curves of base and varying number of passes FSP applied samples

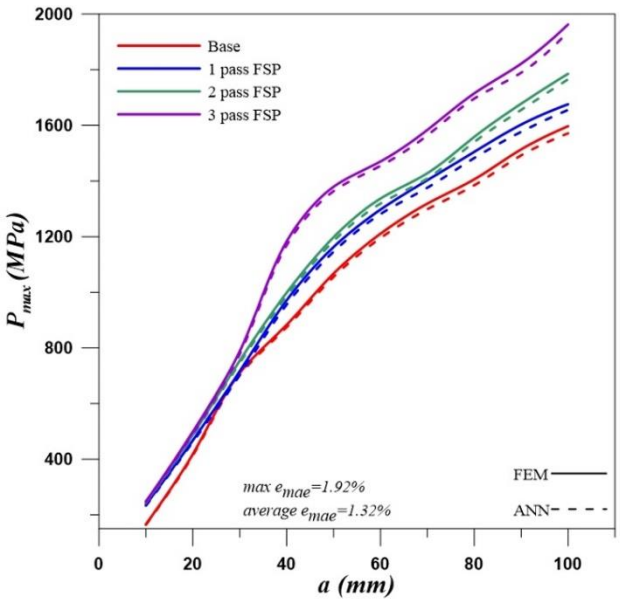

Fig. 9 Maximum contact stress changing with length of distributed load

comprehensive finite element method (FEM) and artificial neural network (ANN), analyses were conducted to elucidate the influence of varying strength and elongation parameters of the material on the maximum contact stress (P_{max}) and contact area (b) corresponding to the length of distributed load (a) and distributed load value (P_0). The average absolute error (average e_{mae}) and maximum absolute error (max e_{mae}) values, which quantify the discrepancies between the outcomes derived from FEM and ANN analyses, were computed by equation number 1 (Nevendra and Singh 2022). The proximity of the e_{mae} values to zero, ranging from 0 to ∞, indicates that reliable and consistent results are achieved between the employed

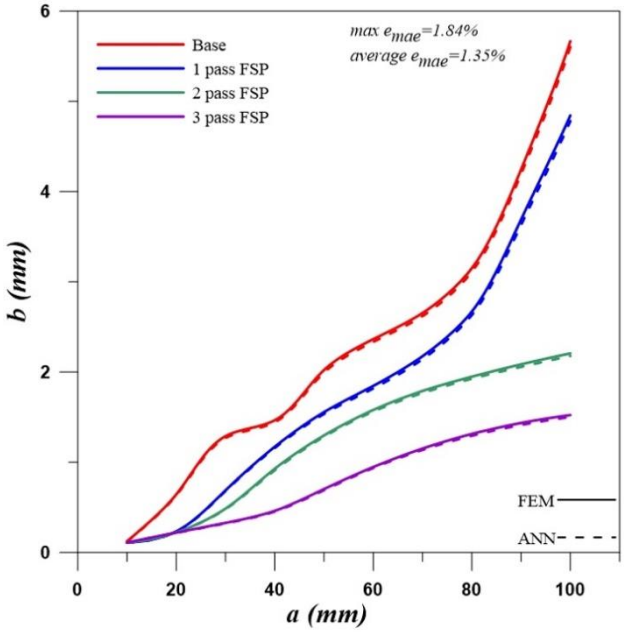

Fig. 10 Contact area changing with length of distributed load

methodologies. Throughout all analyses conducted in this investigation, it is evident that the e_{mae} ratios of the results from FEM and ANN remain below 2%, thereby confirming that the findings derived from both analytical approaches exhibit a high degree of consistency.

$$e_{MAE} = \left| \frac{R_{E_i} - R_{FEM_i \text{ or } MLP_i}}{R_{E_i}} \right| \text{x100}, \quad (i = 1, 2, 3, ..., n) \tag{1}$$

In this study, the predictive success of ANN was compared with the results obtained from FEM. The application of artificial neural networks to predict contact stress and contact area was investigated. The ANN architecture was tested for a single hidden layer and a varying number of neurons from 1 to 16 in this layer. Networks with sos error terms produced superior results. The best of the networks are shown in Table 3. The results showed that the constructed network successfully estimated the contact stresses and contact area and provided a fast and accurate estimation.

Fig. 9 illustrates the fluctuation of maximum contact stress concerning the length of the distributed load, specifically in scenarios where the material characteristics pertinent to the contact problem are conveyed before the FSP and after the FSP across varying passes. As can be seen, the maximum contact stress values increased due to the increasing strength values after the increasing number of FSP passes. The reason for this situation is the relatively high carrying capacity and deformation resistance that

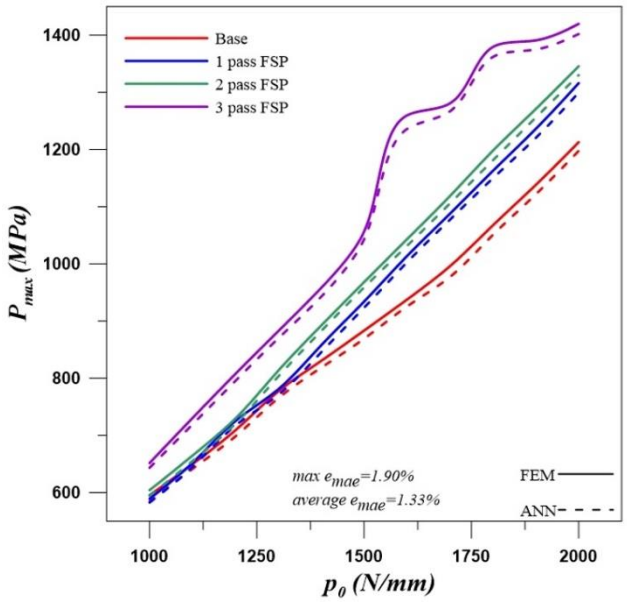

Fig. 11 Maximum contact stress changing with applied distributed load

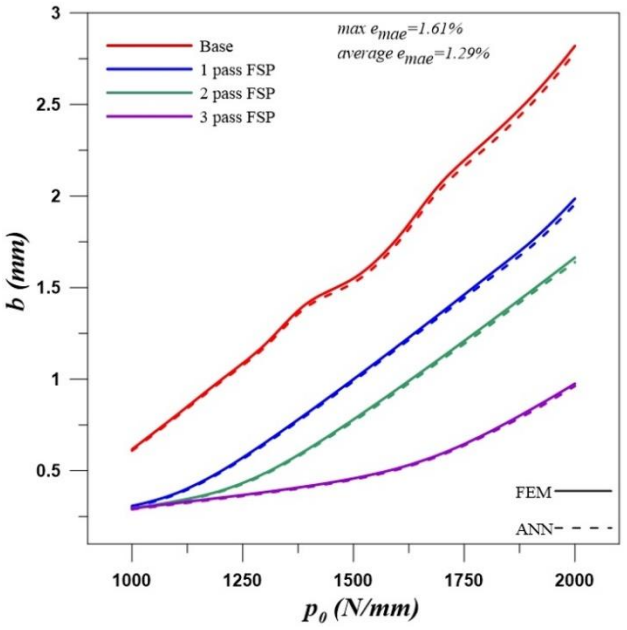

Fig. 12 Contact area changing with applied distributed load

occurs in the structure after increasing material strength values. On the other hand, higher stress concentrations occurred in the structure due to the increased distributed load width, and the maximum stress values also increased.

Fig. 10 depicts the variation of contact area values relative to the distributed load length, particularly when material properties relevant to the contact issue are communicated before and after the FSP. As can be seen from the figure, the contact area values decreased with increasing FSP pass. This situation is because the increasing material strength values after increasing FSP make plastic deformation difficult. On the other hand, as expected, as the distributed load length increased, the contact area values increased due to the increased contact between the surfaces.

Fig. 11 illustrates the maximum contact stress values concerning the distributed load, especially material properties pertinent to the contact problem before and after the FSP. As can be seen, the maximum contact stress values at all changing distributed load values increased in parallel with the increasing strength values after FSP. This situation is because the amount of load the structure can carry increases with increasing strength values of the material. On the other hand, as expected, it can be seen from the figure that the maximum contact stress increases with the increasing amount of distributed load.

Fig. 12 shows the variation of contact area values with applied distributed load in cases where the material properties in the contact problem are transferred before and after FSP. As can be seen from the figure, increasing strength values with an increasing number of passes caused a relative decrease in contact area values. It is thought that the main reason for this situation is that the plastic deformation that occurs during contact decreases relatively after the increasing strength value of the material. On the other hand, as the applied distributed load increased, the amount of surface in contact increased as expected during contact, and as a result, the contact area values increased.

4. Conclusions

FSP was applied to DP 800 steel in varying numbers of passes (1 pass, 2 passes, and 3 passes), and the effects of FSP on the microstructure and mechanical properties were examined. On the other hand, the effects of the strength and elongation change in the material after FSP on the maximum contact stress and contact area at changing distributed load length and distributed load value were examined with FEM and ANN analyses. The data obtained as a result of the investigations are summarized below:

1- The maximum temperatures in the SZ and HAZ attained 874°C and 400°C, respectively, during the FSP.

2- The complex microstructure such as martensite, ferrite, and bainite formed after multi-pass FSP is determined by the initial microstructure, peak temperature, cooling rate, and deformation rate during the process.

3- The hardness value of the base material, which was 220 Hv, increased to 440 Hv after 1 pass of FSP, to 450 Hv after 2 passes of FSP, and to 560 Hv after 3 passes of FSP.

4- Yield and tensile strength values improved from 567 MPa and 829 MPa in the base material to 803 MPa and 968 MPa after one pass of FSP, 907 MPa, and 1038 MPa after two passes, and 1221 MPa and 1407 MPa after three passes. Conversely, the uniform elongation value of 15% in pre-process samples diminished to 6.8% after one pass of FSP, 4.3% after two passes, and 3.2% after three passes.

5- FEM and ANN analyses revealed that maximum contact stress values rose with enhanced strength post-FSP, while contact area values decreased in inverse correlation to strength increases.

References

Abubaker, H.M., Merah, N., Al-Badour, F.A., Albinmousa, J. and Sorour, A.A. (2020), “Influence of Friction Stir Processing on

Mechanical Behavior of 2507 SDSS", *Metals*, **10**(3), 369. https://doi.org/10.3390/met10030369.

Adetunla, A. and Akinlabi, E. (2018), "Mechanical characterization of Al/Ti-6Al-4V surface composite fabricated via FSP: a comparison of tool geometry and number of passes", *Mater. Res. Express*, **5**(11), 115015. https://doi.org/10.1088/2053-1591/aadce5.

Aktarer, S., Küçükömeroğlu, T. and Davut, K. (2019), "Friction stir processing of dual phase steel: Microstructural evolution and mechanical properties", *Mater. Charact.*, **155**, 109787. https://doi.org/10.1016/j.matchar.2019.109787.

Aktarer, S.M., Acar, D. and Küçükomeroğlu, T. (2024), "Effect of friction stir process on hole expansion behavior of dual phase steel", *J. Mater. Eng. Perform.*, **33**, 7020-7039. https://doi.org/10.1007/s11665-023-08565-2.

Al-Furjan, M.S.H., Shan, L., Shen, X., Kolahchi, R. and Rajak, D.K. (2022a), "Combination of FEM-DQM for nonlinear mechanics of porous GPL-reinforced sandwich nanoplates based on various theories", *Thin-Walled Structures*, **178**, 109495. https://doi.org/10.1016/j.tws.2022.109495.

Al-Furjan, M.S.H., Xu, M. X., Farrokhian, A., Jafari, G.S., Shen, X. and Kolahchi, R. (2022b), "On wave propagation in piezoelectric-auxetic honeycomb-2D-FGM micro-sandwich beams based on modified couple stress and refined zigzag theories", *Waves Random Complex Med.*, 1-25. https://doi.org/10.1080/17455030.2022.2030499.

Al-Furjan, M.S.H., Yang, Y., Farrokhian, A., Shen, X., Kolahchi, R. and Rajak, D.K. (2022c), "Dynamic instability of nanocomposite Piezoelectric- leptadenia pyrotechnica rheological elastomer-porous functionally graded materials micro viscoelastic beams at various strain gradient higher-order theories", *Polym. Compos.*, **43**(1), 282-298. https://doi.org/10.1002/pc.26373.

Amirafshar, A. and Pouraliakbar, H. (2015), "Effect of tool pin design on the microstructural evolutions and tribological characteristics of friction stir processed structural steel", *Measurement*, **68**, 111-116. https://doi.org/10.1016/j.measurement.2015.02.051.

Ammarullah, M.I. (2025), "Integrating finite element analysis in total hip arthroplasty for childhood hip disorders: Enhancing precision and outcomes", *World J. Orthop.*, **16**(1). https://doi.org/10.5312/wjo.v16.i1.98871.

Ammarullah, M.I., Hartono, R., Supriyono, T., Santoso, G., Sugiharto, S. and Permana, M.S. (2023), "Polycrystalline diamond as a potential material for the hard-on-hard bearing of total hip prosthesis: von mises stress analysis", *Biomedicines*, **11**(3), 951. https://doi.org/10.3390/biomedicines11030951.

An, X., Lin, Q., Sha, G., Huang, M., Ringer, S., Zhu, Y. and Liao, X. (2016), "Microstructural evolution and phase transformation in twinning-induced plasticity steel induced by high-pressure torsion", *Acta Mater.*, **109**, 300-313. https://doi.org/10.1016/j.actamat.2016.02.045.

Arora, H.S., Ayyagari, A., Saini, J., Selvam, K., Riyadh, S., Pole, M., Grewal, H.S. and Mukherjee, S. (2019), "High tensile ductility and strength in dual-phase bimodal steel through stationary friction stir orocessing", *Sci. Rep.*, **9**(1), 1-6. https://doi.org/10.1038/s41598-019-38707-3.

Bagheri, B. and Abbasi, M. (2020), "Development of AZ91/SiC surface composite by FSP: effect of vibration and process parameters on microstructure and mechanical characteristics", *Adv. Manuf.*, **8**, 82-96. https://doi.org/10.1007/s40436-019-00288-9.

Belabed, Z., Tounsi, A., Bousahla, A.A., Tounsi, A. and Yaylacı, M. (2024), "Accurate free and forced vibration behavior prediction of functionally graded sandwich beams with variable cross-section: A finite element assessment", *Mech. Based Des. Struct.*, 1-34. https://doi.org/10.1080/15397734.2024.2337914.

Chandra, H., Ammarullah, M.I., Marwani, M., Ellyanie, E., Warizal, W., Aditya, D., Pratiwi, D.K. and Utami, N. P.E. (2024), "Preventing environmental and health problems due to LPG transport tank leaks: Fatigue and crack behavior of heat-treated steel investigation", *Cogent Eng.*, **11**(1), 2304491. https://doi.org/10.1080/23311916.2024.2304491.

Costa, M., Verdera, D., Vieira, M. and Rodrigues, D. (2014), "Surface enhancement of cold work tool steels by friction stir processing with a pinless tool", *Appl. Surf. Sci.*, **296**, 214-220. https://doi.org/10.1016/j.apsusc.2014.01.094.

Daikh, A.A., Drai, A., Belarbi, M.O., Houari, M.S.A., Aour, B., Eltaher, M.A. and Mohamed, N.A. (2024), "Static bending response of axially randomly oriented functionally graded carbon nanotubes reinforced composite nanobeams", *Adv. Nano Res.*, **16**(3), 289-301. https://doi.org/10.12989/ANR.2024.16.3.289.

Darabi, A., Chamani, H.R., Kadkhodapour, J., Anaraki, A.P., Alaie, A. and Ayatollahi, M.R. (2017), "Micromechanical analysis of two heat-treated dual phase steels: DP800 and DP980", *Mech. Mater.*, **110**, 68-83. https://doi.org/10.1016/j.mechmat.2017.04.009.

Demirtas, M. and Sekban, D.M. (2021), "Optimization of strength, ductility and wear resistance of low-carbon grade A shipbuilding steel by post-ECAP annealing", *Metall. Res. Technol.*, **118**(2), 217. https://doi.org/10.1051/metal/2021021.

Drai, A., Daikh, A.A., Belarbi, M.O., Houari, M.S.A., Aour, B., Hamdi, A. and Eltaher, M.A. (2023), "Bending of axially functionally graded carbon nanotubes reinforced composite nanobeams", *Adv. Nano Res.*, **14**(3), 211-224. https://doi.org/10.12989/ANR.2023.14.3.211.

Farooq, U., Khan, I., Asif, M., Hira, F., Hussain, G., Ullah, A., Ahmad, S.M., Umar, M., Alhassan, M.A. (2020), "Investigation on the effects of the processing parameters and the number of passes on the flexural properties of polymer nanocomposite fabricated through FSP method", *Mater. Res. Express*, **7**(5), 055310. https://doi.org/10.1088/2053-1591/ab9524.

Furjan, M., Cai, J.X., Shan, L., Shen, X., Yaylacı, M., Rabani bidgoli, M. and Kolahchi, R. (2024a), "Numerical fatigue damage analysis and mathematical modeling of articular cartilage under cyclic load via hyperelasticity theory", *Appl. Math. Model.*, **136**, 115613. https://doi.org/10.1016/j.apm.2024.07.020

Furjan, M., Kolahchi, R. and Yaylacı, M. (2024b), "RFOR-DQHFEM: Hybrid relaxed first-Order reliability and differential quadrature hierarchical finite element method for multi-physics reliability analysis of conical shells", *Thin-Walled Struct.*, **205**, 112583. https://doi.org/10.1016/j.tws.2024.112583

Furjan, M., Kolahchi, R. and Yaylacı, M. (2025), "Energy harvesting capabilities and bandgaps of locally resonant piezoelectric metamaterial panels with self-extraction synchronized circuit", *Appl. Math. Model.*, **141**, 115934. https://doi.org/10.1016/j.apm.2025.115934

Ghalehbandi, S.M., Malaki, M. and Gupta, M. (2018), "Accumulative Roll Bonding—A Review", *Appl. Sci.*, **9**(17), 3627. https://doi.org/10.3390/app9173627.

Gotawala, N., Wadighare, A. and Shrivastava, A. (2020), "Phase transformation during friction stir processing of dual-phase 600 steel", *J. Mater. Sci.*, **55**, 4464-4477. https://doi.org/10.1007/s10853-019-04270-5.

Güvercin, Y., Yaylacı, M., Dizdar, A., Özdemir, M.E., Ay, S., Yaylacı, E.U., Karahasanoğlu, U., Uygun, H. and Peker, G. (2025), "Biomechanical analysis and solution suggestions of screw replacement scenarios in femoral neck fracture surgeries: finite element method", *Orthop Surg.*, **17**, 614-623. https://doi.org/10.1111/os.14337.

Yemenoglu, H., Beder, M., Yaylacı, M., Dizdar, A., Alkurt, M., Naralan, M.E., Uzun Yaylacı, E., Özdemir, M.E., Öztürk, Ş. and

Yeşil, Z. (2025), "Evaluation of prostheses retained zygomatic and dental implants in large defects in the maxilla due to tumors or major trauma by biomechanical 3- dimensional finite element analysis", *BMC Oral Health*, **25**, 99. https://doi.org/10.1186/s12903-025-05468-7

Hajian, M., Abdollah-zadeh, A., Rezaei-Nejad, S., Assadi, H., Hadavi, S., Chung, K. and Shokouhimehr, M. (2015), "Microstructure and mechanical properties of friction stir processed AISI 316L stainless steel", *Mater. Des.*, **67**, 82-94. https://doi.org/10.1016/j.matdes.2014.10.082.

Hajmohammad, H., Ahmad Farrokhian, M. and Kolahchi, R. (2021), "Dynamic analysis in beam element of wave-piercing catamarans undergoing slamming load based on mathematical modelling", *Ocean Eng.*, **234**, 109269. https://doi.org/10.1016/j.oceaneng.2021.109269.

Hashemi, R. and Hussain, G. (2015), "Wear performance of Al/TiN dispersion strengthened surface composite produced through friction stir process: A comparison of tool geometries and number of passes", *Wear*, **324-325**, 45-54. https://doi.org/10.1016/j.wear.2014.11.024.

Hazra, S.S., Gazder, A.A., Carman, A. and Pereloma, E.V. (2011), "Effect of cold rolling on as-ECAP interstitial free steel", *Metall. Mater. Trans. A*, **42**, 1334-1348. https://doi.org/10.1007/s11661-010-0535-5.

Huang, C., Yang, G., Gao, Y., Wu, S. and Zhang, Z. (2008), "Influence of processing temperature on the microstructures and tensile properties of 304L stainless steel by ECAP", *Mater. Sci. Eng. A*, **485**(1-2), 643-650. https://doi.org/10.1016/j.msea.2007.08.067.

Jamaati, R., Toroghinejad, M.R., Edris, H. and Salmani, M.R. (2014), "Fracture of steel nanocomposite made using accumulative roll bonding", *Mater. Sci. Technol.*, **30**(15), 1973-1982. https://doi.org/10.1179/1743284714Y.0000000634.

Kang, H.C., Park, B.J., Jang, J.H., Jang, K.S. and Lee, K.J. (2016), "Determination of the continuous cooling transformation diagram of a high strength low alloyed steel", *Met. Mater. Int.*, **22**, 949-955. https://doi.org/10.1007/s12540-016-6269-1.

Keerthiveettil Ramakrishnan, S., Vijayananth, K., Arivendan, A. and Ammarullah, M.I. (2024), "Evaluating the effects of pineapple fiber, potato waste filler, surface treatment, and fiber length on the mechanical properties of polyethylene composites for biomedical applications", *Results Eng.*, **24**, 102974. https://doi.org/10.1016/j.rineng.2024.102974.

Kolahchi, R., Hosseini H., Hosein Fakhar M., Taherifar R. and Mahmoudi M. (2019), "A numerical method for magneto-hygro-thermal postbuckling analysis of defective quadrilateral graphene sheets using higher order nonlocal strain gradient theory with different movable boundary conditions", *Comput. Math. Appl.*, **78**(6), 2018-34. https://doi.org/10.1016/j.camwa.2019.03.042.

Kolahchi, R., Safari M. and Esmailpour M. (2016), "Dynamic stability analysis of temperature-dependent functionally graded CNT-reinforced visco-plates resting on orthotropic elastomeric medium", *Compos. Struct.*, **150**, 255-65. https://doi.org/10.1016/j.compstruct.2016.05.023.

Küçükömeroğlu T. and Aktarer S.M. (2017), "Microstructure, microhardness and tensileproperties of FSWed DP 800 steel", *J. Achiev. Mater. Manuf. Eng.*, **2**(81), 56-60. https://doi.org/10.5604/01.3001.0010.2038.

Lafi, D.E., Bouhadra, A., Mamen, B., Menasria, A., Bourada, M., Bousahla, A.A., Bourada, F., Tounsi, A. and Yaylaci, M. (2024), "Combined influence of variable distribution models and boundary conditions on the thermodynamic behavior of FG sandwich plates lying on various elastic foundations", *Struct. Eng. Mech.*, **89**(2) 103-119. https://doi.org/10.12989/sem.2024.89.2.103.

Lamura, M.D.P., Ammarullah, M.I., Maula, M.I., Hidayat, T., Bayuseno, A.P. and Jamari, J. (2024), "The Effect of Load, Diameter Ratio, and Friction Coefficient on Residual Stress in a Hemispherical Contact for Application in Biomedical Industry", *J. Mater. Eng. Perform.*, **33**(15), 7528-7536. https://doi.org/10.1007/s11665-024-09330-9.

Merah, N., Abdul Azeem, M., Abubaker, H.M., Albinmousa, J. and Sorour, A.A. (2020), "Friction stir processing influence on microstructure, mechanical, and corrosion behavior of steels: A review", *Materials*, **14**(17), 5023. https://doi.org/10.3390/ma14175023.

Miles, M.P., Pew, J., Nelson, T.W. and Li, M. (2006), "Comparison of formability of friction stir welded and laser welded dual phase 590 steel sheets", *Sci. Technol. Weld. Join.*, **11**(4), 384-388. https://doi.org/10.1179/174329306X107737.

Motezaker, M., Kolahchi R., Kumar Rajak D. and Mahmoud S.R. (2021), "Influences of fiber reinforced polymer layer on the dynamic deflection of concrete pipes containing nanoparticle subjected to earthquake load", *Polym. Compos.*, **42**(8), 4073-81. https://doi.org/10.1002/pc.26118.

Müller, T., Kapp, M., Bachmaier, A., Felfer, P. and Pippan, R. (2019), "Ultrahigh-strength low carbon steel obtained from the martensitic state via high pressure torsion", *Acta Mater.*, **166**, 168-177. https://doi.org/10.1016/j.actamat.2018.12.028.

Nene, S.S., Liu, K., Frank, M., Mishra, R.S., Brennan, R.E., Cho, K.C., Li, Z. and Raabe, D. (2017), "Enhanced strength and ductility in a friction stir processing engineered dual phase high entropy alloy", *Sci. Rep.*, **7**(1), 1-7. https://doi.org/10.1038/s41598-017-16509-9.

Nevendra, M. and Singh, P.A (2022), "Survey of software defect prediction based on deep learning", *Arch. Computat. Methods Eng.*, **29**, 5723-5748. https://doi.org/10.1007/s11831-022-09787-8.

Özdemir, Ö., Ural, H. and de Macêdo Wahrhaftig, A. (2024), "Static stability and vibration response of rotating carbon-nanotube-reinforced composite beams in thermal environment", *Adv. Nano Res.*, **16**(5), 445-458. https://doi.org/10.12989/.2024.16.5.445.

Rathee, S., Maheshwari, S., Noor Siddiquee, A., Srivastava, M. and Kumar Sharma, S. (2015), "Process parameters optimization for enhanced microhardness of AA 6061/ SiC surface composites fabricated via Friction Stir Processing (FSP)", *Mater. Today Proc.*, **3**(10), 4151-4156. https://doi.org/10.1016/j.matpr.2016.11.089.

Salaha, Z.F.M., Ammarullah, M.I., Abdullah, N.N.A.A., Aziz, A.U.A., Gan, H.S., Abdullah, A.H., Abdul Kadir, M.R. and Ramlee, M.H. (2023), "Biomechanical Effects of the Porous Structure of Gyroid and Voronoi Hip Implants: A Finite Element Analysis Using an Experimentally Validated Model", *Materials*, **16**(9), 3298. https://doi.org/10.3390/ma16093298.

Saravanan, R., Arunachalam, S.J., Sathish, T., Giri, J. and Ammarullah, M.I. (2025), "Influence of Silane-Treated Jute/ Kenaf Fibers on the Mechanical Properties of Polymer Composites for Biomedical Applications: Optimization Using RSM and ANN Approaches", *Eng. Rep.*, **7**(1), e13059. https://doi.org/10.1002/eng2.13059.

Sekban, D., Saray, O., Aktarer, S., Purcek, G. and Ma, Z. (2015), "Microstructure, mechanical properties and formability of friction stir processed interstitial-free steel", *Mater. Sci. Eng. A*, **642**, 57-64. https://doi.org/10.1016/j.msea.2015.06.068.

Sekban, D.M., Aktarer, S.M., Zhang, H. Xue, P., Ma, Z. and Purcek, G. (2017), "Microstructural and mechanical evolution of a low carbon steel by friction stir processing", *Metall. Mater. Trans. A*, **48**, 3869-3879. https://doi.org/10.1007/s11661-017-4157-z.

Sekban, D.M., Uzun Yaylacı, E., Özdemir, M.E., Öztürk, Ş., Yaylacı, M. and Panda, S.K. (2024a), "Formability behavior of AH-32 shipbuilding steel strengthened by friction stir process",

Theor. Appl. Fract. Mech., **132**, 104485. https://doi.org/10.1016/j.tafmec.2024.104485.

Sekban, D.M., Uzun Yaylacı, E., Özdemir, M.E., Yaylacı, M. and Tounsi, A. (2024b), "Investigating formability behavior of friction stir-welded high-strength shipbuilding steel using experimental, finite element, and artificial neural network methods", *J. Mater. Eng. Perform.* https://doi.org/10.1007/s11665-024-09501-8.

Sekban, D.M., Yaylacı, E.U., Özdemir, M.E., Yaylacı, M. (2024c), "Determination of formability behavior of steel used in ships by various methods", *Struct. Eng. Mech.*, **92**(2), 189-96. https://doi.org/10.12989/SEM.2024.92.2.189.

Sekban, D.M. and Ölmez, H. (2021), "Effect of stress-strain curve changing with equal channel angular pressing on ultimate strength of ship hull stiffened panels", *Struct. Eng. Mech.*, **78**(4), 473-84. https://doi.org/10.12989/SEM.2021.78.4.473.

Sen, B., Bhowmik, A., Prakash, C. and Ammarullah, M.I. (2024), "Prediction of specific cutting energy consumption in eco-benign lubricating environment for biomedical industry applications: Exploring efficacy of GEP, ANN, and RSM models", *AIP Adv.*, **14**(8), 085216. https://doi.org/10.1063/5.0217508.

Senthilkumar, R., Prakash, M., Arun, N. and Jeyakumar, A.A. (2019), "The effect of the number of passes in friction stir processing of aluminum alloy (AA6082) and its failure analysis", *Appl. Surf. Sci.*, **491**, 420-431. https://doi.org/10.1016/j.apsusc.2019.06.132.

Shan, L., Furjan, M., Kolahchi, R. and Yaylacı, M. (2025), "Optimization flutter response of laminated smart nano-composite truncated conical shell under supersonic aerodynamic pressure using hybrid IGWO-DQHFEM", *Aerosp. Sci. Technol.*, **156**. https://doi.org/10.1016/j.ast.2024.109766

Shen, X., Li, T., Xu, L., Kiarasi, F., Babaei, M. and Asemi, K. (2024), "Free vibration analysis of FG porous spherical cap reinforced by graphene platelet resting on Winkler foundation", *Adv. Nano Res.*, **16**(1), 11-16. https://doi.org/10.12989/anr.2024.16.1.011.

Tauviqirrahman, M., Ammarullah, M.I., Jamari, J., Saputra, E., Winarni, T.I., Kurniawan, F.D., Shiddiq, S.A. and Van Der Heide, E. (2023), "Analysis of contact pressure in a 3D model of dual-mobility hip joint prosthesis under a gait cycle", *Sci. Rep.*, **13**(1), 3564. https://doi.org/10.1038/s41598-023-30725-6.

Tlija, M., Rashid, T., Sana, M., Farooq, M.U., Ammarullah, M.I. (2024), "AISI D2 steel machining and manufacturing process optimization for tooling applications in biomedical industry", *AIP Adv.*, **14**(10), 105129. https://doi.org/10.1063/5.0217712.

Tonelli, L., Morri, A., Toschi, S., Shaaban, M., Ammar, H.R., Ahmed, M.M.Z., Ramadan, R.M., El-Mahallawi I. and Ceschini L. (2019), "Effect of FSP parameters and tool geometry on microstructure, hardness, and wear properties of AA7075 with and without reinforcing B4C ceramic particles", *Int. J. Adv. Manuf. Technol.*, **102**, 3945-3961. https://doi.org/10.1007/s00170-019-03442-6.

Trung, N.D., Huy, D.T.N., Bokov, D.O., Opulencia, M.J.C., Alsaikhan, F., Ahmad, I. and Karlibaeva, G. (2023), "Synergistic bond properties of new steel fibers with rounded-end from carbon nanotubes reinforced ultra-high performance concrete matrix", *Adv. Nano Res.*, **14**(4), 363-373. https://doi.org/10.12989/ANR.2023.14.4.363.

Uzun Yaylacı, E. (2024), "Application of artificial neural network for the mechano-bactericidal effect of bioinspired nanopatterned surfaces", *Eur. Biophys. J.*, **53**(7), 415-427. https://doi.org/10.1007/s00249-024-01723-x.

Uzun Yaylacı, E., Özdemir, M.E., Güvercin, Y., Öztürk, Ş. and Yaylacı, M. (2023a), "Analysis of the mechano-bactericidal effects of nanopatterned surfaces on implant-derived bacteria using the FEM", *Adv. Nano Res.*, **15**(6), 567-577. https://doi.org/10.12989/anr.2023.15.6.567.

Uzun Yaylacı, E., Yaylacı, M., Özdemir, M.E., Terzi, M. and Öztürk, Ş. (2023b), "Analyzing the mechano-bactericidal effect of nano-patterned surfaces by finite element method and verification with artificial neural networks", *Adv. Nano Res.*, **15**(2), 165-174. https://doi.org/10.12989/anr.2023.15.2.165.

Wang, X., Guo, X., Babaei, M., Fili, R. and Farahani, H. (2023), "Natural frequency analysis of joined conical-cylindrical-conical shells made of graphene platelet reinforced composite resting on Winkler elastic foundation", *Adv. Nano Res.*, **15**(4), 367-384. https://doi.org/10.12989/anr.2023.15.4.367.

Wetscher, F., Pippan, R., Sturm, S., Scheu, C. and Dehm, G. (2006), "TEM investigations of the structural evolution in a pearlitic steel deformed by high-pressure torsion", *Metall. Mater. Trans. A*, **37**, 1963-1968. https://doi.org/10.1007/s11661-006-0138-3.

Wu, X. (2023), "Nonlinear finite element vibration analysis of functionally graded nanocomposite spherical shells reinforced with graphene platelets", *Adv. Nano Res.*, **15**(2), 141-153. https://doi.org/10.12989/anr.2023.15.2.141.

Xia, L., Wang, R., Chen, G., Asemi, K. and Tounsi, A. (2023), "The finite element method for dynamics of FG porous truncated conical panels reinforced with graphene platelets based on the 3-D elasticity", *Adv. Nano Res.*, **14**(4), 375-389. https://doi.org/10.12989/ANR.2023.14.4.375.

Xue, P., Li, W., Wang, D., Wang, W., Xiao, B. and Ma, Z. (2016), "Enhanced mechanical properties of medium carbon steel casting via friction stir processing and subsequent annealing", *Mater. Sci. Eng. A*, **670**, 153-158. https://doi.org/10.1016/j.msea.2016.06.014.

Yaylacı, M., Yaylı, M., Öztürk, Ş., Ay, S., Özdemir, M.E., Uzun Yaylacı, E. and Birinci, A. (2024a), "Examining the contact problem of a functionally graded layer supported by an elastic half-plane with the analytical and numerical methods", *Math. Meth. Appl. Sci.*, **47**, 10400-10420 https://doi.org/10.1002/MMA.10129

Yaylacı, M., Öner, E., Adıyaman, G., Öztürk, Ş., Uzun Yaylacı, E. and Birinci, A., (2024b), "Analyzing of continuous and discontinuous contact problems of a functionally graded layer: theory of elasticity and finite element method", *Mech. Based Des. Struct. Mech.*, **52**(8), 5720-5738. https://doi.org/10.1080/15397734.2023.2262562

Yaylacı, M., Uzun Yaylacı, E., Turan, M., Özdemir, M. E., Öztürk, Ş. and Ay, S. (2024c), "Research of the crack problem of a functionally graded layer", *Steel Compos. Struct.*, **50**(1), 77-87. https://doi.org/10.12989/scs.2024.50.1.077

Yilmaz, M., Ozturk Yilmaz, I. and Saray, O. (2024), "Fatigue and impact behavior of friction stir processed dual-phase (DP600) steel sheets", *Metals*, **14**(3), 305. https://doi.org/10.3390/met14030305.

Yılmaz, S., Fırat, M., Ateş, A. and Özdemir, Ö. (2022), "Analyzing the economic water loss level with a discrete stochastic optimization algorithm by considering budget constraints", *Aqua Water Infrastruct. Ecosyst. Soc.*, **71**(7), 835-848. https://doi.org/10.2166/aqua.2022.060

AT